*nanomaterials*

MDPI

*Communication*

# Nanotoxicity of $ZrS_3$ Probed in a Bioluminescence Test on *E. coli* Bacteria: The Effect of Evolving $H_2S$

**Olga V. Zakharova [1,2], Alexander A. Gusev [1,2,*], Jehad Abourahma [3], Nataliia S. Vorobeva [3], Dmitry V. Sokolov [2], Dmitry S. Muratov [2], Denis V. Kuznetsov [2] and Alexander Sinitskii [3,4,*]**

1 Research Institute for Environmental Science and Biotechnology, Derzhavin Tambov State University, Tambov 392000, Russia; olgazakharova1@mail.ru
2 Department of Functional Nanosystems and High-Temperature Materials, National University of Science and Technology "MISIS", Moscow 119991, Russia; triplplay@bk.ru (D.V.S.); muratov@misis.ru (D.S.M.); dk@misis.ru (D.V.K.)
3 Department of Chemistry, University of Nebraska—Lincoln, Lincoln, NE 68588, USA; jabourahma@huskers.unl.edu (J.A.); nataliia.vorobeva@huskers.unl.edu (N.S.V.)
4 Nebraska Center for Materials and Nanoscience, University of Nebraska—Lincoln, Lincoln, NE 68588, USA
* Correspondence: nanosecurity@mail.ru (A.A.G.); sinitskii@unl.edu (A.S.); Tel.: +7-910-756-4546 (A.A.G.); +1-402-472-3543 (A.S.)

Received: 24 June 2020; Accepted: 8 July 2020; Published: 18 July 2020


**Abstract:** Materials from a large family of transition metal trichalcogenides (TMTCs) attract considerable attention because of their potential applications in electronics, optoelectronics and energy storage, but information on their toxicity is lacking. In this study, we investigated the toxicity of $ZrS_3$, a prominent TMTC material, toward photoluminescent *E. coli* bacteria in a bioluminescence test. We found that freshly prepared $ZrS_3$ suspensions in physiological saline solution with concentrations as high as 1 g/L did not exhibit any toxic effects on the bacteria. However, $ZrS_3$ suspensions that were stored for 24 h prior to the bioluminescence tests were very toxic to the bacteria and inhibited their emission, even at concentrations down to 0.001 g/L. We explain these observations by the aqueous hydrolysis of $ZrS_3$, which resulted in the formation of $ZrO_x$ on the surface of $ZrS_3$ particles and the release of toxic $H_2S$. The formation of $ZrO_x$ was confirmed by the XPS analysis, while the characteristic $H_2S$ smell was noticeable for the 24 h suspensions. This study demonstrates that while $ZrS_3$ appears to be intrinsically nontoxic to photoluminescent *E. coli* bacteria, it may exhibit high toxicity in aqueous media. The results of this study can likely be extended to other transition metal chalcogenides, as their toxicity in aqueous solutions may also increase over time due to hydrolysis and the formation of $H_2S$. The results of this study also demonstrate that since many systems involving nanomaterials are unstable and evolve over time in various ways, their toxicity may evolve as well, which should be considered for relevant toxicity tests.

**Keywords:** zirconium trisulfide; nanotoxicity; antibacterial properties; bioluminescence test; *Escherichia coli*

## 1. Introduction

In recent years, much effort has been devoted to investigating various two-dimensional materials, such as graphene, hexagonal boron nitride, transition metal dichalcogenides, MXenes and many others [1–3]. Many of these materials show promise for a great variety of applications in numerous fields, including electronics, optoelectronics, composites and energy storage. With the increasing prospect of incorporation of 2D materials in very diverse consumer applications, a great deal of recent research has been focused on the assessment of their potential toxicity [4]. Understanding of the potential toxic effects associated with 2D materials is also important in the view of their widely

discussed biomedical applications, which include bioimaging [5], drug delivery [6], phototherapy [7], biosensors [8] and many others.

While a considerable number of in vitro and in vivo studies have focused on the assessment of toxicity of graphene-based materials [9,10], other 2D materials have received much less attention from researchers. For example, there have been no nanotoxicity studies of materials from a large family of transition metal trichalcogenides (TMTCs) with the general formula $MX_3$ (M = Ti, Zr, Hf, Nb or Ta; X = S, Se or Te) [11–14], which have recently received much attention due to their promising electronic [15–20] and optoelectronic [21,22] and thermoelectric properties [23–25]. The crystal structure of TMTC materials is different from other 2D materials, which is shown in Figure 1a using $ZrS_3$ as an example [11–14,26]. This structure can be viewed as composed of 1D chains of $ZrS_3$ trigonal prisms, in which the $Zr^{4+}$ centers are surrounded by the sulfide ($S^{2-}$) and disulfide ($S_2^{2-}$) species. The 1D chains then assemble into 2D layers through weak van der Waals-like interactions, while the layers stack into bulk crystals (Figure 1a). Because of their highly anisotropic structure, exfoliation of TMTC crystals into both 2D layers and 1D chains is possible [26].

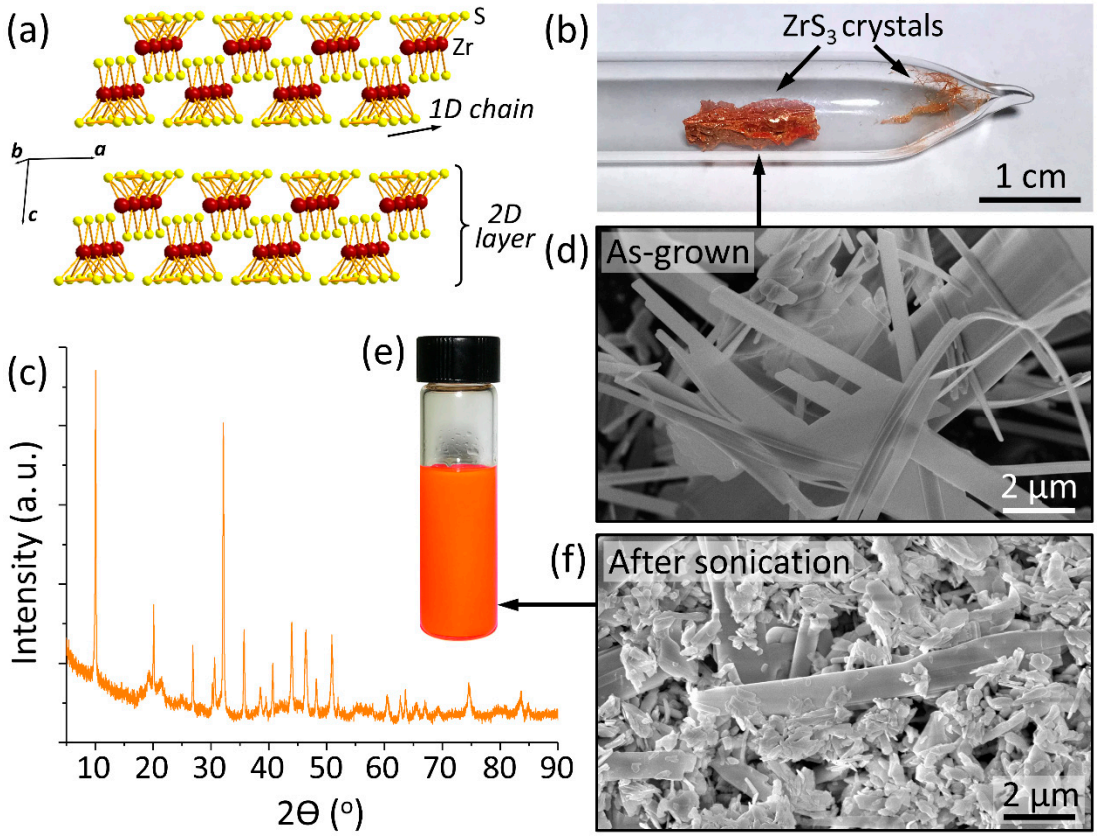


**Figure 1.** (**a**) Crystal structure of $ZrS_3$ ($P\,2_1/m$ space group); (**b**) optical photograph of an evacuated quartz ampule with orange $ZrS_3$ crystals indicated by the arrows; (**c**) XRD spectrum of $ZrS_3$ crystals; (**d**) SEM image of the as-grown $ZrS_3$ crystals shown by the arrow in panel b; (**e**) optical photograph of a vial with 1 g/L suspension of exfoliated $ZrS_3$ crystals, which were dispersed in PS solution by sonication; (**f**) SEM image of $ZrS_3$ particles after sonication in PS solution.

While no TMTC has been a subject of nanotoxicity studies, this work was specifically focused on $ZrS_3$, which was shown theoretically and experimentally to be a promising material for charge transport layers in perovskite light-emitting diodes [27], battery cathodes [28], nonlinear optics [29], photovoltaics and photocatalysis [30]. Furthermore, the results of a recent angle-resolved photoluminescence study suggested that because of its highly anisotropic band structure [31] and emission properties $ZrS_3$ could be potentially employed in biomedical applications [32]. The breadth of possible applications of

$ZrS_3$, including those potentially involving living organisms, warrants nanotoxicity studies of this emerging 2D material. Here, we investigated the effect of $ZrS_3$ dispersed in physiological (PS) solution on photoluminescent *Escherichia coli* (*E. coli*) bacteria using a bioluminescence test [33–37].

The bioluminescence test is a highly standardized method that was employed in numerous nanotoxicity studies [33–38]. It is based on monitoring the intensity of emission of photoluminescent bacteria, such as *Vibrio fischeri*, in the presence of toxic substances. The bioluminescence intensity decreases proportionally to the inhibition of bacteria that directly correlates to toxicity. For aqueous suspensions of $ZrS_3$ nanoparticles we found that their toxicity to photoluminescent *E. coli* bacteria strongly depends on the time between suspension preparation and bioluminescence test. In freshly prepared suspensions the $ZrS_3$ nanoparticles did not exhibit any toxicity even at concentrations up to 1 g/L. However, if suspensions were stored for 24 h prior to the tests, toxic effects were observed at concentrations down to 0.001 g/L. We explain this observation by the slow hydrolysis of $ZrS_3$ in aqueous media that is accompanied by an evolution of highly toxic $H_2S$.

This study demonstrates that $ZrS_3$, while initially nontoxic to photoluminescent *E. coli* bacteria, starts exhibiting appreciable toxicity over time if kept in an aqueous medium. The results of this study can likely be extended to other transition metal chalcogenides, as their toxicity in aqueous solutions may also increase over time due to hydrolysis and the formation of $H_2S$. The results of this study also demonstrate that since many systems involving nanomaterials are unstable and evolve over time in various ways, their toxicity may evolve as well, which should be considered for relevant toxicity tests.

## 2. Materials and Methods

All chemicals were purchased from Sigma-Aldrich (USA) unless noted otherwise. $ZrS_3$ crystals were grown by the direct reaction of stoichiometric amounts of Zr metal and S vapor in an evacuated quartz ampule at 800 °C for 48 h, as described in our previous work [39]. The crystals were characterized by X-ray diffraction (XRD) using a PANalytical Empyrean diffractometer (Netherlands) with Cu K$\alpha$ radiation. Scanning electron microscopy (SEM) of $ZrS_3$ crystals was performed using a FEI Nova NanoSEM 450 scanning electron microscope (USA) at the accelerating voltage of 5 kV. Raman spectroscopy was performed using a Thermo Scientific DXR Raman microscope (USA) with a 532 nm excitation laser and a 100× objective. XPS analysis was performed at room temperature using a Thermo Scientific K-Alpha X-ray photoelectron spectrometer (USA) with a monochromatic Al K$\alpha$ (1486.6 eV) X-ray source and a low energy electron flood gun for charge compensation. High-resolution XPS spectra of Zr*3d* and S*2p* were collected using a pass energy of 20 eV and a 0.1 eV step. To collect XPS spectra of pristine $ZrS_3$, as-grown crystals were cleaved in air directly before introduction into the loading vacuum chamber to minimize the contribution of surface contamination. XPS spectra of solution-exfoliated $ZrS_3$ crystals were recorded on samples produced by drying droplets of the corresponding suspensions in air.

To prepare $ZrS_3$ suspensions for nanotoxicity experiments, $ZrS_3$ crystals were sonicated in physiological saline solution (PS; 9 g/L NaCl aqueous solution) for 20 min to produce a homogeneous orange suspension with a concentration of 1 g/L. Other suspensions were prepared by diluting this $ZrS_3$ stock suspension to concentrations of 0.0001, 0.001, 0.01 and 0.1 g/L. The nanotoxicity experiments were performed on freshly prepared $ZrS_3$ suspensions, which were analyzed less than 0.5 h after preparation and the suspensions that were stored for 24 h prior to the measurements.

The laboratory glassware for sample storage and biotesting was soaked in a mixture of potassium bichromate and sulfuric acid for about 3 h, then washed with deionized (DI) water, deacidified with a sodium bicarbonate solution and finally washed four times with DI water and dried in an oven.

The toxicity of $ZrS_3$ suspensions was measured by a bioluminescence technique that is generally used for the assessment of toxic effects of nanomaterials. The procedure was similar to the widely used bioluminescence inhibition test with *Vibrio fischeri* [33–37]. We monitored changes in intensity of bioluminescence of genetically modified photoluminescent *E. coli* bacteria in the presence of $ZrS_3$

nanoparticles or other tested chemicals compared to the emission of a control sample (same bacteria in a pure PS solution).

We used commercial recombinant *E. coli* K12 TG1 bacteria modified with *luxCDABE* genes of photoluminescent *Photobacterium leiognathi* 54D10 marine bacteria. Lyophilized *E. coli* K12 TG1 bacteria under the brand name Ecolum were purchased from NVO ImmunoTek (Russian Federation). Before the nanotoxicity experiments, the lyophilized bacteria were rehydrated in a PS solution at 4 °C for 30 min and then at room temperature for 1 h. The solutions used in this study had an *E. coli* concentration of about $2.5 \times 10^7$ cells/mL. In a typical bioluminescence experiment, 0.1 mL of this *E. coli* solution was mixed with 0.9 mL of a $ZrS_3$ suspension in PS. The resulting mixture was stored for 30 min prior to the measurements, which were performed using a NIKI MLT Biotox-10 luminometer (Russian Federation). The instrument detected bioluminescence of bacteria in the 300–600 nm spectral range with the maximum detector sensitivity between 380 and 490 nm. Parallel measurements of the studied and control samples were carried out. The control samples were prepared by diluting 0.1 mL of the *E. coli* stock solution with 0.9 mL of PS.

We compared the toxicity of $ZrS_3$ with that of zirconyl chloride ($ZrOCl_2 \cdot 8H_2O$), a common zirconium compound. Both compounds contain $Zr^{4+}$, but while $ZrS_3$ is practically insoluble in water and was present in the PS suspensions as partially exfoliated particles, zirconyl chloride is water soluble. We prepared 0.000172, 0.00172, 0.0172, 0.172 and 1.72 g/L solutions of $ZrOCl_2 \cdot 8H_2O$ in PS, which matched the 0.0001, 0.001, 0.01, 0.1 and 1 g/L $ZrS_3$ suspensions, respectively, in zirconium concentrations. Then, 0.9 mL aliquots of zirconyl chloride solutions were mixed with 0.1 mL aliquots of the *E. coli* stock solution, and the resulting mixtures were stored for 30 min and used in bioluminescence experiments.

For the positive control we used sodium dichloroisocyanurate ($C_3Cl_2N_3NaO_3$, SDC), a compound with well-known toxicity that is widely used as an efficient disinfectant against Gram-positive and Gram-negative bacteria, viruses and fungi [40]. We prepared 0.0001, 0.001, 0.01, 0.1 and 1 g/L solutions of SDC in PS, and then, 0.9 mL aliquots of these solutions were mixed with 0.1 mL aliquots of the *E. coli* stock solution. The resulting mixtures were stored for 30 min and used in bioluminescence experiments. As in the experiments with $ZrS_3$, the bioluminescence tests with $ZrOCl_2$ and SDC involved control samples prepared by diluting 0.1 mL aliquots of the *E. coli* stock solution with 0.9 mL aliquots of PS.

Each bioluminescence experiment was performed at least 5 times, and the averaged results are presented.

## 3. Results and Discussion

Figure 1b shows an optical photograph of a reaction ampule after the $ZrS_3$ growth, which was performed through a direct reaction between a Zr foil and sulfur vapor at 800 °C. While some crystals form on the quartz surface (Figure 1b), most of the $ZrS_3$ grows directly on a foil forming a spongy material comprising disordered $ZrS_3$ nanobelt crystals. This material was highly crystalline, as illustrated by the XRD spectrum in Figure 1c. The peaks in the XRD spectrum are narrow and sharp, and their positions agree well with prior literature reports for $ZrS_3$ crystals [27,31,39,41]. A representative SEM image of the $ZrS_3$ crystals is shown in Figure 1d. The crystals had a nanobelt shape, which reflects their quasi-1D crystal structure (Figure 1a) with the *b* crystallographic direction of 1D chains corresponding to the long axes of the crystals. Most of the as-grown $ZrS_3$ crystals were over 10 μm long. Figure 1e shows an optical photograph of a uniform orange suspension of exfoliated $ZrS_3$ crystals in PS (1 g/L) that was used for the toxicity experiments. After the sonication, the average crystal size decreased, which is illustrated by the SEM image in Figure 1f (note that the SEM images of $ZrS_3$ crystals before and after sonication are shown in panels d and f, respectively, at the same magnification). While some $ZrS_3$ crystals retained their nanobelt shape, others were split by sonication into randomly shaped particles with sizes of about 1 μm.

The results of bioluminescence experiments are summarized in Figure 2. In both panels the emission of the control sample (*E. coli* in a pure PS solution) is indicated by the green dashed lines at 3754 pulses/s. As expected, SDC exhibited a strong toxic effect on *E. coli* bacteria, which showed

decreased photoluminescence compared to the control sample for all SDC concentrations (Figure 2). The decrease in the bacterial activity was proportional to the SDC concentration.

For the zirconium compounds compared in this study, $ZrS_3$ was generally less toxic than $ZrOCl_2$ at all concentrations, regardless of whether the solutions were stored for 30 min or 24 h prior to their mixing with *E. coli* bacteria. In both cases, the $ZrOCl_2$ solutions strongly suppressed the bacterial activities at concentrations above 0.01 g/L (Figure 2). The higher toxicity of $ZrOCl_2$ compared to $ZrS_3$, especially for the freshly prepared solutions (Figure 2a), can be explained by its solubility in aqueous media. Even though all these samples contained same amounts of zirconium, in the solutions of water-soluble $ZrOCl_2$ all Zr(IV) was available for interaction with the bacteria in a form of aqueous complexes. On the contrary, since $ZrS_3$ is insoluble in water most Zr(IV) in the suspensions was in the bulk of $ZrS_3$ particles and thus did not directly interact with the bacteria.

The toxic effects were very different for the $ZrS_3$ suspensions that were stored for 30 min or 24 h prior to their mixing with the bacteria. Freshly prepared $ZrS_3$ suspensions did not exhibit any toxicity to the photoluminescent *E. coli* bacteria across the entire tested concentration range (Figure 2a). In fact, for all studied concentrations we observed a considerable stimulating activity of $ZrS_3$ nanoparticles on the bioluminescence of *E. coli*, as all emission values were higher than for the control sample at 3754 pulses/s. However, the $ZrS_3$ suspensions that were stored for 24 h prior to the experiment suppressed the bioluminescence of *E. coli* even at a concentration as low as 0.001 g/L (Figure 2b), indicating their high toxicity.

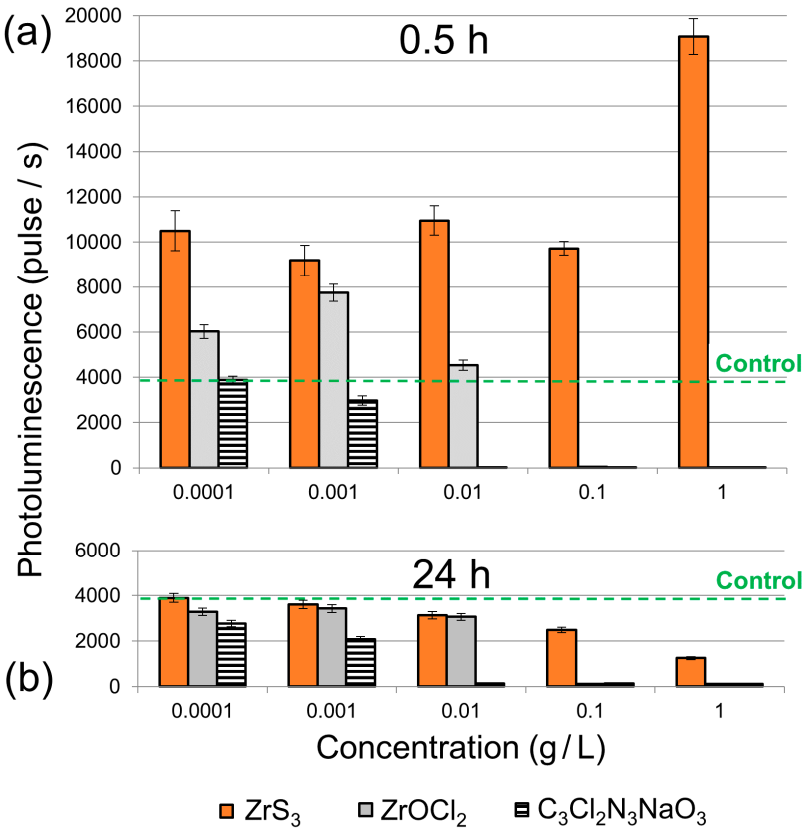


**Figure 2.** *E. coli* luminescence values in (**a**) as-prepared (0.5 h) and (**b**) 24 h solutions of $ZrS_3$, $ZrOCl_2$ and $C_3Cl_2N_3NaO_3$. For $ZrOCl_2$ solutions, the concentrations were 0.000172, 0.00172, 0.0172, 0.172 and 1.72 g/L, so that they matched the 0.0001, 0.001, 0.01, 0.1 and 1 g/L $ZrS_3$ suspensions in the zirconium concentrations, respectively.

It should be noted that the $ZrS_3$ suspensions that were stored for 24 h produced a mild but noticeable smell of $H_2S$, which can form as a result of aqueous hydrolysis of $ZrS_3$. Because of its

well-known toxic effects, hydrogen disulfide forming in aqueous $ZrS_3$ suspensions over time could be responsible for their increased toxicity. Since the hydrolysis of $ZrS_3$ is accompanied by the formation of zirconium oxide ($ZrO_x$) on the surface of nanoparticles, we investigated this process using XPS (Figure 3).

Figure 3a shows XPS Zr*3d* spectra of pristine $ZrS_3$ crystals and the $ZrS_3$ nanoparticles stored in an aqueous medium for 24 h. The top spectrum shows two peaks located at 181.16 eV and 183.55 eV, both of which can be assigned to $ZrS_3$ [42]. The XPS Zr*3d* spectrum of the $ZrS_3$ nanoparticles stored in an aqueous medium can be deconvoluted into two doublet peaks. In addition to the same doublet found in pristine $ZrS_3$, the bottom spectrum in Figure 3a also shows the $Zr3d_{3/2}$ and $Zr3d_{5/2}$ components of $ZrO_x$ at 182.52 eV and 184.95 eV, respectively. The spin-orbit doublet splittings for $ZrS_3$ and $ZrO_x$ are 2.39 eV and 2.43 eV, respectively [43]. Thus, these spectra confirm the formation of $ZrO_x$ on the surface of $ZrS_3$ nanoparticles. The XPS S*2p* spectrum contains signals from sulfur located in the sulfide ($S^{2-}$) and disulfide ($S_2^{2-}$) species. The spectrum shown in Figure 3b was fitted using two doublet peaks. The binding energies of $S2p_{1/2}$ and $S2p_{3/2}$ for the sulfide are 161.55 eV and 162.65 eV, respectively. The disulfide group peaks are located at 162.76 eV and 163.85 eV. The intensity ratio of two sulfur components is a characteristic value for $ZrS_3$ and should be equal to 2. The calculated ratio of the fitted $S_2^{2-}/S^{2-}$ peaks is 1.85, which is in good agreement with literature data [42].

We also compared the as-grown $ZrS_3$ crystals with the solution-exfoliated $ZrS_3$ nanoparticles by Raman spectroscopy, see the inset in Figure 3b. The Raman spectrum of pristine $ZrS_3$ crystals confirms their high quality and crystallinity, showing very sharp and well-resolved peaks at about 148, 277, 317 and 526 $cm^{-1}$ in accordance with previous studies [32,44]. The spectrum of $ZrS_3$ nanoparticles from a freshly prepared suspension is nearly identical to that of the as-grown crystals, demonstrating that while the sonication decreased the average size of particles (see Figure 1d,f), their structure and crystallinity were not much affected. The Raman spectrum of $ZrS_3$ nanoparticles from a suspension that was stored for 24 h prior to the measurements also looks very similar to the other two spectra (see the inset in Figure 3b). While XPS, a surface-sensitive method, demonstrated the formation of $ZrO_x$ on the surface of $ZrS_3$ nanoparticles, Raman spectroscopy shows that in bulk they retained their properties.

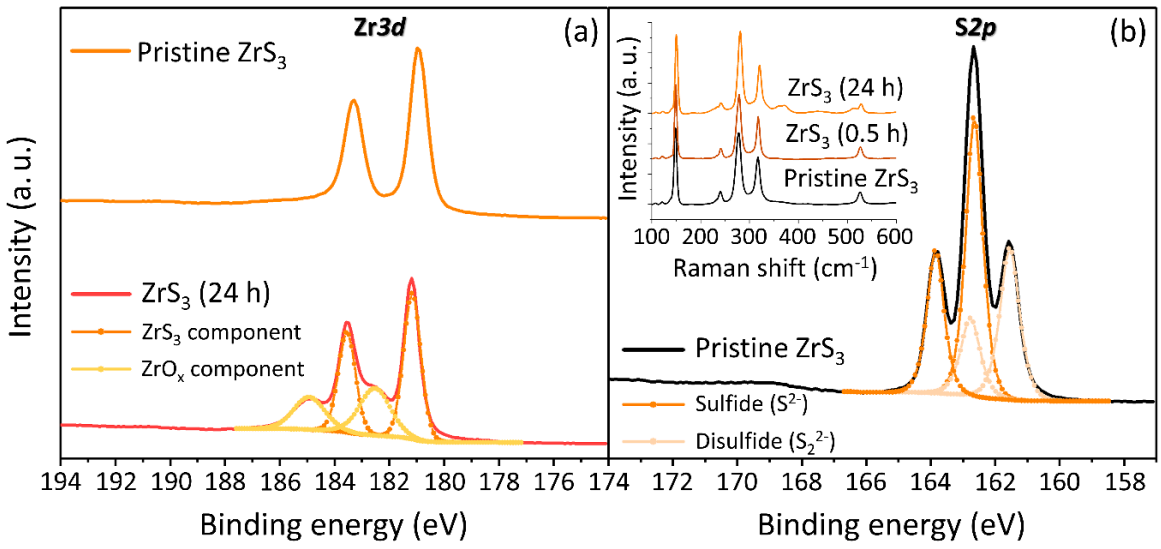


**Figure 3.** Spectroscopic characterization of $ZrS_3$ crystals before and after sonication. (**a**) Comparison of XPS Zr*3d* spectra of pristine $ZrS_3$ crystals (top) and $ZrS_3$ nanoparticles stored in water for 24 h (bottom); (**b**) XPS S*2p* spectrum of pristine $ZrS_3$. Inset shows Raman spectra of pristine $ZrS_3$ crystals, $ZrS_3$ nanoparticles from a freshly prepared suspension (0.5 h), and $ZrS_3$ nanoparticles stored in an aqueous medium for 24 h.

The XPS results confirm the formation of $ZrO_x$ due to the aqueous hydrolysis of $ZrS_3$, which is accompanied by the evolution of $H_2S$. It is plausible that toxic $H_2S$ is responsible for the increased toxicity of $ZrS_3$ suspensions stored for 24 h (Figure 2b). The increased bioluminescence observed for the freshly prepared $ZrS_3$ suspensions could also be related to the formation $H_2S$ that is initially formed in very small quantities. Other studies reported that low concentrations of hydrogen disulfide may exhibit stimulation of bacteria and protect them against oxidative stress [45,46], which is a common toxicity mechanism for nanoparticles. As the $H_2S$ concentration increases over the 24 h storage period, the $ZrS_3$ suspensions become highly toxic to bacteria, which we observed experimentally.

## 4. Summary

This work reports the first nanotoxicity study of materials from a large TMTC family. More specifically, we investigated the toxicity of $ZrS_3$, a prominent TMTC material, toward photoluminescent *E. coli* bacteria in a bioluminescence test. We investigated the solution exfoliation of $ZrS_3$ and prepared aqueous suspensions of $ZrS_3$ nanoparticles with concentrations ranging from 0.0001 to 1 g/L. We found that freshly prepared $ZrS_3$ suspensions with concentrations as high as 1 g/L did not exhibit any toxic effects on the bacteria and, on the contrary, stimulated their activity. However, $ZrS_3$ suspensions that were stored for 24 h prior to the bioluminescence tests were very toxic to the bacteria and inhibited their emission even at concentrations down to 0.001 g/L. We explain these observations by the aqueous hydrolysis of $ZrS_3$, which resulted in the formation of $ZrO_x$ on the surface of nanoparticles and the release of toxic $H_2S$. The formation of $ZrO_x$ was confirmed by the XPS analysis, while the characteristic $H_2S$ smell was noticeable for the 24 h suspensions. Hydrogen disulfide could be responsible for the bacterial stimulation in the freshly prepared $ZrS_3$ suspensions, because at small concentrations $H_2S$ was shown to protect bacteria against oxidative stress [45,46], which is widely regarded as a common nanoparticle-induced toxicity mechanism. However, as more $H_2S$ was released during the hydrolysis of $ZrS_3$ over a 24 h period, the suspensions became toxic to the bacteria.

This study demonstrates that $ZrS_3$ suspensions, while initially nontoxic to photoluminescent *E. coli* bacteria, start exhibiting appreciable toxicity over time. The results of this study can likely be extended to other transition metal chalcogenides, as their toxicity in aqueous solutions may also increase over time due to hydrolysis and the formation of $H_2S$. The results of this study also demonstrate that since many systems involving nanomaterials are unstable and evolve over time in various ways, their toxicity may evolve as well, which should be considered for relevant toxicity tests.

**Author Contributions:** Conceptualization, O.V.Z., A.A.G. and A.S.; formal analysis, O.V.Z., J.A., N.S.V., D.V.S., D.S.M., A.A.G. and A.S.; investigation, O.V.Z., J.A., N.S.V., D.V.S., D.S.M., A.A.G.; supervision, A.A.G., D.V.K. and A.S.; writing–original draft, A.A.G., O.V.Z. and A.S.; writing–review & editing, O.V.Z., J.A., N.S.V., D.S.M., D.V.K., A.A.G. and A.S. All authors have read and agreed to the published version of the manuscript.

**Funding:** The nanotoxicity experiments were supported by the Ministry of Education and Science of the Russian Federation through grant K2-2020-014. The research on the synthesis and characterization of $ZrS_3$ employed the instrumentation at the Nebraska Nanoscale Facility, which is supported by Nebraska Research Initiative and the National Science Foundation (NSF) through ECCS-1542182.

**Conflicts of Interest:** The authors declare no conflicts of interest.

## References

1. Geim, A.K.; Grigorieva, I.V. Van der Waals heterostructures. *Nature* **2013**, *499*, 419–425. [CrossRef]
2. Butler, S.Z.; Hollen, S.M.; Cao, L.; Cui, Y.; Gupta, J.A.; Gutiérrez, H.R.; Heinz, T.F.; Hong, S.S.; Huang, J.; Ismach, A.F.; et al. Progress, challenges, and opportunities in two-dimensional materials beyond graphene. *ACS Nano* **2013**, *7*, 2898–2926. [CrossRef]
3. Bhimanapati, G.R.; Lin, Z.; Meunier, V.; Jung, Y.; Cha, J.; Das, S.; Xiao, D.; Son, Y.; Strano, M.S.; Cooper, V.R.; et al. Recent advances in two-dimensional materials beyond graphene. *ACS Nano* **2015**, *9*, 11509–11539. [CrossRef]
4. Tan, E.; Li, B.L.; Ariga, K.; Lim, C.-T.; Garaj, S.; Leong, D.T. Toxicity of two-dimensional layered materials and their heterostructures. *Bioconj. Chem.* **2019**, *30*, 2287–2299. [CrossRef]

5. Xu, S.; Li, D.; Wu, P. One-pot, facile, and versatile synthesis of monolayer $MoS_2/WS_2$ quantum dots as bioimaging probes and efficient electrocatalysts for hydrogen evolution reaction. *Adv. Funct. Mater.* **2015**, *25*, 1127–1136. [CrossRef]
6. Yin, W.; Yan, L.; Yu, J.; Tian, G.; Zhou, L.; Zheng, X.; Zhang, X.; Yong, Y.; Li, J.; Gu, Z.; et al. High-throughput synthesis of single-layer $MoS_2$ nanosheets as a near-infrared photothermal-triggered drug delivery for effective cancer therapy. *ACS Nano* **2014**, *8*, 6922–6933. [CrossRef] [PubMed]
7. Chou, S.S.; Kaehr, B.; Kim, J.; Foley, B.M.; De, M.; Hopkins, P.E.; Huang, J.; Brinker, C.J.; Dravid, V.P. Chemically exfoliated $MoS_2$ as near-infrared photothermal agents. *Angew. Chem. Int. Ed.* **2013**, *52*, 4160–4164. [CrossRef] [PubMed]
8. Ha, H.D.; Han, D.J.; Choi, J.S.; Park, M.; Seo, T.S. Dual role of blue luminescent $MoS_2$ quantum dots in fluorescence resonance energy transfer phenomenon. *Small* **2014**, *10*, 3858–3862. [CrossRef] [PubMed]
9. Seabra, A.B.; Paula, A.J.; de Lima, R.; Alves, O.L.; Durán, N. Nanotoxicity of graphene and graphene oxide. *Chem. Res. Toxicol.* **2014**, *27*, 159–168. [CrossRef] [PubMed]
10. Bianco, A. Graphene: Safe or toxic? The two faces of the medal. *Angew. Chem. Int. Ed.* **2013**, *52*, 4986–4997. [CrossRef] [PubMed]
11. Furuseth, S.; Brattas, L.; Kjekshus, A. On the crystal structures of $TiS_3$, $ZrS_3$, $ZrSe_3$, $ZrTe_3$, $HfS_3$, and $HfSe_3$. *Acta Chem. Scan. A* **1975**, *29*, 623–631. [CrossRef]
12. Srivastava, S.K.; Avasthi, B.N. Preparation, structure and properties of transition metal trichalcogenides. *J. Mater. Sci.* **1992**, *27*, 3693–3705. [CrossRef]
13. Dai, J.; Li, M.; Zeng, X.C. Group IVB transition metal trichalcogenides: A new class of 2D layered materials beyond graphene. *Wiley Interdiscip. Rev. Comput. Mol. Sci.* **2016**, *6*, 211–222. [CrossRef]
14. Island, J.O.; Molina-Mendoza, A.J.; Barawi, M.; Biele, R.; Flores, E.; Clamagirand, J.M.; Ares, J.R.; Sánchez, C.; van der Zant, H.S.; D'Agosta, R.; et al. Electronics and optoelectronics of quasi-1D layered transition metal trichalcogenides. *2D Mater.* **2017**, *4*, 022003. [CrossRef]
15. Island, J.O.; Barawi, M.; Biele, R.; Almazán, A.; Clamagirand, J.M.; Ares, J.R.; Sánchez, C.; van der Zant, H.S.J.; Álvarez, J.V.; D'Agosta, R.; et al. $TiS_3$ transistors with tailored morphology and electrical properties. *Adv. Mater.* **2015**, *27*, 2595–2601. [CrossRef]
16. Lipatov, A.; Wilson, P.M.; Shekhirev, M.; Teeter, J.D.; Netusil, R.; Sinitskii, A. Few-layered titanium trisulfide ($TiS_3$) field-effect transistors. *Nanoscale* **2015**, *7*, 12291–12296. [CrossRef]
17. Molina-Mendoza, A.J.; Island, J.O.; Paz, W.S.; Clamagirand, J.M.; Ares, J.R.; Flores, E.; Leardini, F.; Sánchez, C.; Agraït, N.; Rubio-Bollinger, G.; et al. High current density electrical breakdown of $TiS_3$ nanoribbon-based field-effect transistors. *Adv. Funct. Mater.* **2017**, *27*, 1605647. [CrossRef]
18. Yi, H.; Komesu, T.; Gilbert, S.; Hao, G.; Yost, A.J.; Lipatov, A.; Sinitskii, A.; Avila, J.; Chen, C.; Asensio, M.C.; et al. The band structure of the quasi-one-dimensional layered semiconductor $TiS_3(001)$. *Appl. Phys. Lett.* **2018**, *112*, 052102. [CrossRef]
19. Gilbert, S.J.; Lipatov, A.; Yost, A.J.; Loes, M.J.; Sinitskii, A.; Dowben, P.A. The electronic properties of Au and Pt metal contacts on quasi-one-dimensional layered $TiS_3(001)$. *Appl. Phys. Lett.* **2019**, *114*, 101604. [CrossRef]
20. Randle, M.; Lipatov, A.; Kumar, A.; Kwan, C.-P.; Nathawat, J.; Barut, B.; Yin, S.; He, K.; Arabchigavkani, N.; Dixit, R.; et al. Gate-controlled metal–insulator transition in $TiS_3$ nanowire field-effect transistors. *ACS Nano* **2019**, *13*, 803–811. [CrossRef]
21. Island, J.O.; Buscema, M.; Barawi, M.; Clamagirand, J.M.; Ares, J.R.; Sánchez, C.; Ferrer, I.J.; Steele, G.A.; van der Zant, H.S.J.; Castellanos-Gomez, A. Ultrahigh photoresponse of few-layer $TiS_3$ nanoribbon transistors. *Adv. Opt. Mater.* **2014**, *2*, 641–645. [CrossRef]
22. Cui, Q.; Lipatov, A.; Wilt, J.S.; Bellus, M.Z.; Zeng, X.C.; Wu, J.; Sinitskii, A.; Zhao, H. Time-resolved measurements of photocarrier dynamics in $TiS_3$ nanoribbons. *ACS Appl. Mater. Interfaces* **2016**, *8*, 18334–18338. [CrossRef] [PubMed]
23. Hayashi, A.; Matsuyama, T.; Sakuda, A.; Tatsumisago, M. Amorphous titanium sulfide electrode for all-solid-state rechargeable lithium batteries with high capacity. *Chem. Lett.* **2012**, *41*, 886–888. [CrossRef]
24. Zhang, J.; Liu, X.; Wen, Y.; Shi, L.; Chen, R.; Liu, H.; Shan, B. Titanium trisulfide monolayer as a potential thermoelectric material: A first-principles-based Boltzmann transport study. *ACS Appl. Mater. Interfaces* **2017**, *9*, 2509–2515. [CrossRef]
25. Morozova, N.V.; Korobeinikov, I.V.; Kurochka, K.V.; Titov, A.N.; Ovsyannikov, S.V. Thermoelectric properties of compressed titanium and zirconium trichalcogenides. *J. Phys. Chem. C* **2018**, *122*, 14362–14372. [CrossRef]

26. Lipatov, A.; Loes, M.J.; Lu, H.; Dai, J.; Patoka, P.; Vorobeva, N.S.; Muratov, D.S.; Ulrich, G.; Kästner, B.; Hoehl, A.; et al. Quasi-1D $TiS_3$ nanoribbons: Mechanical exfoliation and thickness-dependent Raman spectroscopy. *ACS Nano* **2018**, *12*, 12713–12720. [CrossRef]
27. Muratov, D.S.; Ishteev, A.R.; Lypenko, D.A.; Vanyushin, V.O.; Gostishev, P.; Perova, S.; Saranin, D.S.; Rossi, D.; Auf der Maur, M.; Volonakis, G.; et al. Slot-die printed two-dimensional $ZrS_3$ charge transport layer for perovskite light-emitting diodes. *ACS Appl. Mater. Interfaces* **2019**, *11*, 48021–48028. [CrossRef]
28. Giagloglou, K.; Payne, J.L.; Crouch, C.; Gover, R.K.B.; Connor, P.A.; Irvine, J.T.S. Zirconium trisulfide as a promising cathode material for Li primary thermal batteries. *J. Electrochem. Soc.* **2016**, *163*, A3126–A3130. [CrossRef]
29. Wu, J.-J.; Tao, Y.-R.; Wang, J.-N.; Wu, Z.-Y.; Fan, L.; Wu, X.-C. Reverse saturable absorption and nonlinear refraction of ultrathin $ZrS_3$ nanobelts. *Nanoscale* **2016**, *8*, 10371–10379. [CrossRef]
30. Abdulsalam, M.; Joubert, D.P. Electronic and optical properties of $MX_3$ (M = Ti, Zr and Hf; X = S, Se) structures: A first principles insight. *Phys. Status Solidi B* **2016**, *253*, 868–874. [CrossRef]
31. Yi, H.; Gilbert, S.J.; Lipatov, A.; Sinitskii, A.; Avila, J.; Abourahma, J.; Komesu, T.; Asensio, M.C.; Dowben, P.A. The electronic band structure of quasi-one-dimensional van der Waals semiconductors: The effective hole mass of $ZrS_3$ compared to $TiS_3$. *J. Phys. Condens. Matter* **2020**, *32*, 29LT01. [CrossRef] [PubMed]
32. Pant, A.; Torun, E.; Chen, B.; Bhat, S.; Fan, X.; Wu, K.; Wright, D.P.; Peeters, F.M.; Soignard, E.; Sahin, H.; et al. Strong dichroic emission in the pseudo one dimensional material $ZrS_3$. *Nanoscale* **2016**, *8*, 16259–16265. [CrossRef] [PubMed]
33. Backhaus, T.; Froehner, K.; Altenburger, R.; Grimme, L.H. Toxicity testing with *Vibrio fischeri*: A comparison between the long term (24 h) and the short term (30 min) bioassay. *Chemosphere* **1997**, *35*, 2925–2938. [CrossRef]
34. Lopes, I.; Ribeiro, R.; Antunes, F.E.; Rocha-Santos, T.A.P.; Rasteiro, M.G.; Soares, A.M.V.M.; Gonçalves, F.; Pereira, R. Toxicity and genotoxicity of organic and inorganic nanoparticles to the bacteria *Vibrio fischeri* and *Salmonella typhimurium*. *Ecotoxicology* **2012**, *21*, 637–648. [CrossRef]
35. Garcia, A.; Recillas, S.; Sánchez, A.; Font, X. The luminescent bacteria test to determine the acute toxicity of nanoparticle suspensions. In *Nanotoxicity: Methods and Protocols*; Reineke, J., Ed.; Humana Press: Totowa, NJ, USA, 2012; pp. 255–259.
36. Mogilnaya, O.A.; Puzyr', A.P.; Bondar', V.S. Growth and bioluminescence of luminous bacteria under the action of aflatoxin B1 before and after its treatment with nanodiamonds. *Appl. Biochem. Microbiol.* **2010**, *46*, 33–37. [CrossRef]
37. Zarubina, A.P.; Lukashev, E.P.; Deev, L.I.; Parkhomenko, I.M.; Rubin, A.B. Biotesting the biological effects of single-wall carbon nanotubes using bioluminescent bacteria test-system. *Nanotechnol. Russ.* **2009**, *4*, 871–875. [CrossRef]
38. Gusev, A.; Zakharova, O.; Muratov, D.S.; Vorobeva, N.S.; Sarker, M.; Rybkin, I.; Bratashov, D.; Kolesnikov, E.; Lapanje, A.; Kuznetsov, D.V.; et al. Medium-dependent antibacterial properties and bacterial filtration ability of reduced graphene oxide. *Nanomaterials* **2019**, *9*, 1454. [CrossRef]
39. Muratov, D.S.; Vanyushin, V.O.; Vorobeva, N.S.; Jukova, P.; Lipatov, A.; Kolesnikov, E.A.; Karpenkov, D.; Kuznetsov, D.V.; Sinitskii, A. Synthesis and exfoliation of quasi-1D $(Zr,Ti)S_3$ solid solutions for device measurements. *J. Alloys Compd.* **2020**, *815*, 152316. [CrossRef]
40. Clasen, T.; Edmondson, P. Sodium dichloroisocyanurate (NaDCC) tablets as an alternative to sodium hypochlorite for the routine treatment of drinking water at the household level. *Int. J. Hyg. Environ. Health* **2006**, *209*, 173–181. [CrossRef]
41. Haraldsen, H.; Rost, E.; Kjekshus, A.; Steffens, A. On properties of $TiS_3$, $ZrS_3$, and $HfS_3$. *Acta Chem. Scand.* **1963**, *17*, 1283–1292. [CrossRef]
42. Jellinek, F.; Pollak, R.A.; Shafer, M.W. X-ray photoelectron spectra and electronic structure of zirconium trisulfide and triselenide. *Mater. Res. Bull.* **1974**, *9*, 845–856. [CrossRef]
43. Crist, B.V. *Handbooks of Monochromatic XPS Spectra. Vol. 2. Commercially Pure Binary Oxides*; XPS International LLC: Mountain View, CA, USA, 2007.
44. Sourisseau, C.; Mathey, Y. The infrared, Raman, resonance Raman spectra and the valence force field of the $ZrS_3$ layer-type compound. *Chem. Phys.* **1981**, *63*, 143–156. [CrossRef]

45. Mironov, A.; Seregina, T.; Nagornykh, M.; Luhachack, L.G.; Korolkova, N.; Lopes, L.E.; Kotova, V.; Zavilgelsky, G.; Shakulov, R.; Shatalin, K.; et al. Mechanism of $H_2S$-mediated protection against oxidative stress in *Escherichia coli*. *Proc. Natl. Acad. Sci. USA* **2017**, *114*, 6022–6027. [CrossRef] [PubMed]
46. Kimura, H. Production and physiological effects of hydrogen sulfide. *Antioxid. Redox Signal.* **2014**, *20*, 783–793. [CrossRef]